International Journal of Rock Mechanics and Mining Sciences 122 (2019) 104033

Contents lists available at ScienceDirect

International Journal of Rock Mechanics and Mining Sciences

journal homepage: www.elsevier.com/locate/ijrmms

Study of automated top-coal caving in extra-thick coal seams using the continuum-discontinuum element method

Qunlei Zhang[a,b], Jinchao Yue[a], Chuang Liu[b], Chun Feng[c], Huamin Li[b,*]

[a] School of Water Conservancy and Environment, Zhengzhou University, Zhengzhou, 450001, China
[b] School of Energy Science and Engineering, Henan Polytechnic University, Jiaozuo, 454003, China
[c] Institute of Mechanics, Chinese Academy of Sciences, Beijing, 100190, China

ARTICLE INFO

Keywords:
Extra-thick coal seam
Automated top-coal caving
Continuum-discontinuum element method
Constitutive model of hydraulic support
Bergmark–Roos model

ABSTRACT

In order to investigate top-coal drawing regularity and automated top-coal caving technology in extra-thick coal seams, an approach coupling the particle element and the block element is presented based on the continuum-discontinuum element method (CDEM). Then, the constitutive model of hydraulic support is introduced into the CDEM to simulate the top-coal drawing process. Meanwhile, the Bergmark–Roos model for coal drawing of single support is extended into the collaborative coal drawing of multiple supports to optimize the automated top-coal caving technology. Finally, CDEM models of hydraulic support, armored face conveyer and coal-rock strata are established according to the field conditions of the "Tongxin Coal Mine". Then, the top-coal drawing mechanism is analyzed, and an automated top-coal caving technology is proposed. The results show that under the interaction between hydraulic support and surrounding rocks, the final drawing body of initial top-coal drawing appears as an irregular, deflected ellipsoid shape. During different support-moving cycles, the coal-rock structure affects the coal drawing amount and support resistance. A statistical comparison of the coal-rock drawing amount based on 100 drawing openings indicates that the standard deviation of the coal drawing amount in automated, one-round coal caving is 1.83 m^2 less than that in traditional coal caving (8.23 m^2), and the coal drawing amount from each drawing window is more uniform. For multi-round coal caving techniques, the average recovery rate remains at 79.4% and the rock mixed rate is less than 1%. Based on a comparison of several coal caving techniques, automated four-round coal caving technology is the optimal technology, in which the change rate of the standard deviation of the coal drawing amount as well as the top-coal recovery rate are both largest.

1. Introduction

In China, the reserve and production of thick seam coals accounts for 45% of underground coal resources and production, and the longwall top-coal caving technique (LTCC) is one of the major mining methods used to extract thick coal seams.[1–3] The technique was first applied in the 1940s in Russia and subsequently used in France, former Yugoslavia, Hungary, Romania, former Czechoslovakia, Turkey and India.[4,5] The LTCC technique has been used in industrial trials and applications in China for more than 30 years, which has gradually entered a mature stage of independent research and innovation.[6] However, the coal drawing termination condition of the traditional top-coal caving technique is "rocks appear, close the opening" (the coal drawing process is allowed to continue until all broken top-coal is recovered and waste rock appears, and then, the tail canopies are lowered and the drawing opening is closed), which is necessary to artificially control the drawing opening, and thus, worker operations are heavy and complex. Currently, top-coal caving mining has begun to develop toward intelligent mining and an automated top-coal caving control system was developed, which realizes automatic mining of the fully mechanized top-coal caving mining face.[7–10] The drawing opening of automated top-coal caving technology is controlled by automated equipment with time as a variable, and the operation is simple and orderly. However, for different coal caving technologies, the difference in the coal drawing amount from each drawing opening affects the transport efficiency of the scraper conveyer. Moreover, the rock mixed rate and top-coal recovery rate also greatly impact the economic benefits of coal mining. Therefore, the investigation of automated top-coal drawing in thick coal seams has important guiding for the development of automated top-coal caving mining.

* Corresponding author.
E-mail address: lihm@hpu.edu.cn (H. Li).

https://doi.org/10.1016/j.ijrmms.2019.04.019
Received 1 August 2018; Received in revised form 17 April 2019; Accepted 29 April 2019
Available online 09 September 2019

Regarding the theory of top-coal drawing, Chinese scholars used the ore-drawing ellipsoidal theory in the early stages and put forward the theory of the coal drawing ellipsoid.[11–13] Because China adopted support with a lower opening at the rear for top-coal drawing after 2000, many scholars have also proposed the loose medium flow field theory, and then, a BBR research system for top-coal caving mining was developed.[14–17] With the development of computer technology, numerical simulation has become an effective means to study the caving mechanism. Yasitli analyzed the top-coal caving mechanism at the Omerler Underground Mine using the finite difference code FLAC^{3D}.[4] Using PFC,^{2D} Xie proved that arch structures can actually be formed during the top-coal caving process under gravity conditions, and vibration can easily destroy the arch structure.[3] Wang studied the top-coal drawing body with PFC^{3D} and determined that the 3D drawing body resembles an ellipsoid. Due to the impact of support, the approximate ellipsoid is incomplete.[18] Yang studied the effects of the upward angle on the drawing mechanism in longwall top-coal caving mining with PFC^{3D}, and the shape of the top-coal terminated boundary becomes steeper with an increasing upward angle.[2] Moreover, a mine-scale analysis of Longwall Top Coal Caving (LTCC) was performed by COSFLOW, and various LTCC parameters were evaluated for a mine.[19] The 2D and 3D numerical models were used to improve the understanding of the caving mechanics, and a new cavability assessment criterion for Longwall Top Coal Caving was also developed, which is included the Top Coal Recovery and (TCR) and the Main Caving Distance (MCD).[20]

Due to the complexity of the top-coal caving mining process in extra-thick coal seams, observations are difficult, and limited data is obtained in the field. Moreover, laboratory experiments can only be used to study the top-coal drawing process under a simplified boundary of the stope. In the existing simulation methods, FLAC3D and COSFLOW can accurately calculate the stress of the intact coal-rock mass but cannot well simulate the fracturing and crushing processes of the coal-rock mass. PFC does not fully consider the effect of intact coal-rock mass on the coal drawing process, and the PFC rigid wall does not truly reflect the interaction between hydraulic support and surrounding rocks. The continuum-discontinuum element method (CDEM) couples the finite element method and the discrete element method, which conducts finite element calculation in the continuous domain and conducts discrete element calculation in the discontinuous domain. Currently, CDEM has been applied in various fields of civil and geotechnical engineering. The simulation results agree well with those of experiment, theoretical analysis and site monitoring. It indicates that based on CDEM, not only the deformation and motion characteristics of the material can be simulated, but also the progressive failure process of the material from the continuous state to the discontinuous state can be well studied.[21–27] Although the automated top-coal caving in extra-thick coal seams is a complex three-dimensional space and time evolution process including coal mining and overburden collapse, based on the continuum-discontinuum element method (CDEM), the interaction between hydraulic support and surrounding rocks can be considered through the coupled calculation of particle element and block element. Moreover, the crushing and drawing processes of top-coal can be simulated using a particle element with an initial strength. In addition, the rock mixed rate, top-coal recovery rate and difference in the coal drawing amount can also be statistically analyzed. However, research regarding the theory and technology of automated top-coal caving in extra-thick coal seams using CDEM has not been reported in the literature.

In July 2016, automated, fully mechanized mining equipment was installed for automated coal mining trials in the Tongxin Coal Mine, with per panel production of more than 10 million tons. Considering the Tongxin Coal Mine with an engineering background, in this paper, brief details of the coupled calculation approach of particle and block elements based on CDEM are presented and verified, and then, the numerical and constitutive models of hydraulic support are established. Meanwhile, the Bergmark–Roos theory is introduced to optimize the automated coal caving technology. The variation regularity of top-coal drawing under the interaction between hydraulic support and surrounding rocks is summarized, and decisive parameters influencing automated top-coal caving technology are optimized through a statistical comparison of the coal-rock drawing amount based on 100 drawing openings. Further, automated top-coal caving technology is proposed through consideration of the rock mixed rate, top-coal recovery rate and the standard deviation of coal drawing amount. Finally, the method of determining automated coal drawing time combining with simulation and in-site test is discussed.

2. Theories of CDEM and top-coal drawing

2.1. Coupled approach of particle and block elements

Top-coal caving mining involves the processes of intact top-coal fracturing, crushing and drawing. The particle element with an initial strength can well simulate the processes of top-coal breaking and moving. The block element can accurately analyze the force and deformation of the load rock strata and hydraulic support. The CDEM is well suited for performing numerical analyses on the coal-rock accumulated state, top-coal drawing process and coal drawing technology. The block, particle and mutual coupling calculation approach of CDEM are presented as follows.

The calculation method is a time-stepping, explicit scheme. CDEM can be used to model static or dynamic problems through dynamic equations of motion:

$$m\ddot{u} + c\dot{u} + F_d + F_k + F_e = 0 \tag{1}$$

where u is the node displacement, m is the nodal mass, $\ddot{u}$ is the node acceleration, c is the damping force coefficient, $\dot{u}$ is the node speed, F_d is the node deformation force, and F_e is the node external force.

The incremental method is used to calculate the stress and deformation of the block element:

$$\begin{aligned} \Delta\xi_i &= B_i \cdot \Delta u \\ \Delta\sigma_i &= D \cdot \Delta\xi_i \\ \sigma_i^n &= \sigma_i^0 + \Delta\sigma_i \\ F_d &= \sum_{i=1}^{N} B_i^T \cdot \sigma_i^n \cdot \omega_i \cdot J_i \end{aligned} \tag{2}$$

where i is the element Gaussian point, $\Delta\xi_i$ is the incremental strain vector, B_i is the strain matrix, Δu is the node incremental displacement vector, $\Delta\sigma_i$ is the incremental stress vector, D is the element elastic matrix, σ_i^n is the total stress at the current step, σ_i^0 is the total stress at the previous step, F_d is the node force vector, N is the number of Gaussian points, ω_i is the integral coefficient, and J_i is the Jacobian determinant value.

To enable the particle element to characterize the properties of the continuous medium, the linked bar model is used to simulate the top-coal caving process from the intact state to the crushed state.[27,28] As indicated in Fig. 1, the linked bar model is similar to the beam element of the finite element method, which is used to transfer the force and moment between two particles in contact. The linked bar model has a

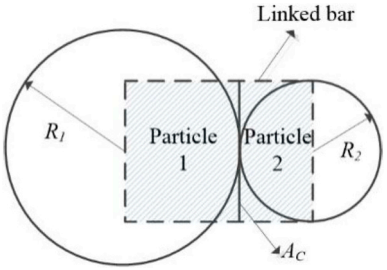

Fig. 1. The linked bar model.

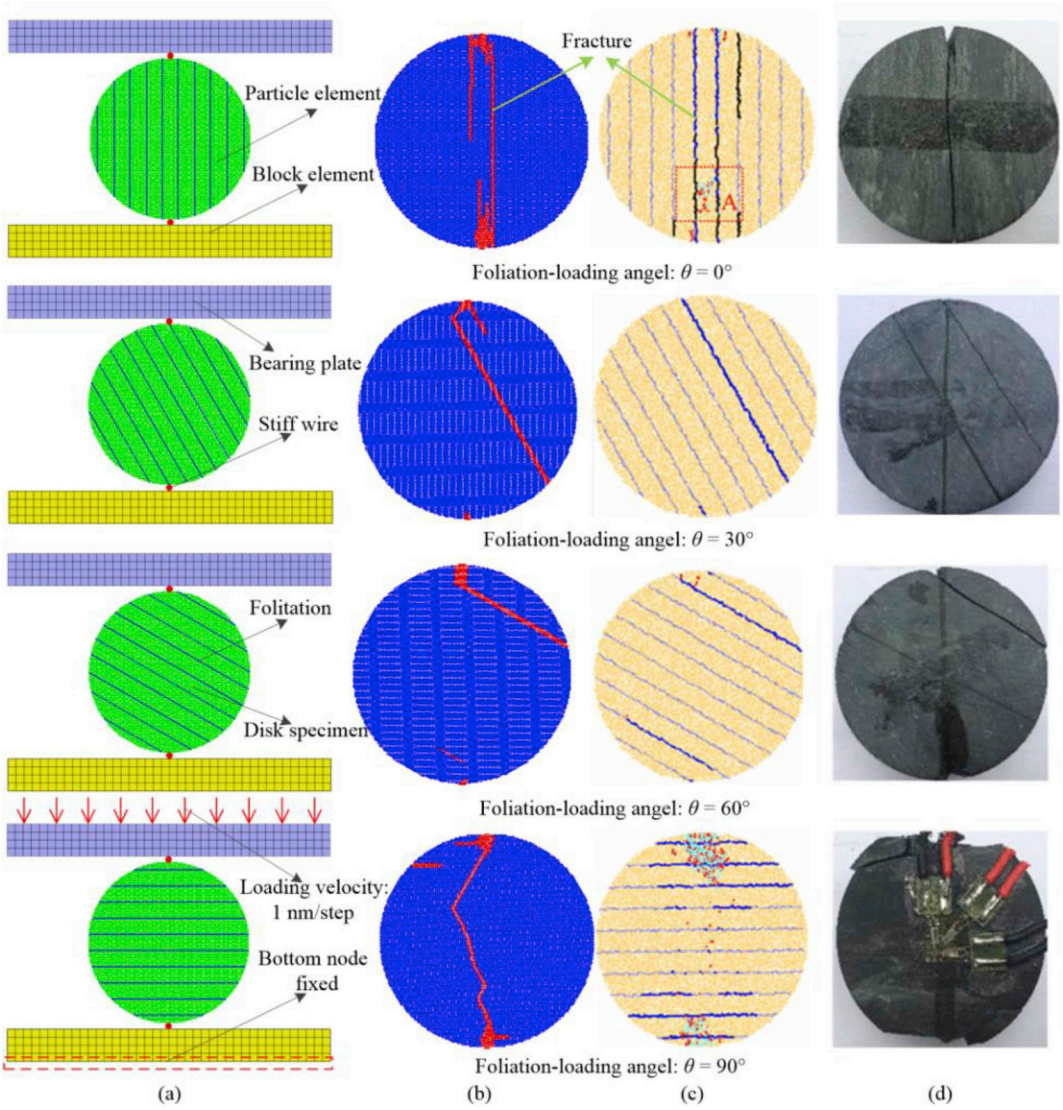

Fig. 2. The Calibration of CDEM: (a) the numerical models; (b) the current work; (c) the simulation results in the reference; and (d) the experimental results in the reference.

certain size and shape, which is a rectangle. One side of the rectangle is the sum of the radius of the two contacting particles, while the other side is the diameter of the smaller particle. The contact between the particles is a face contact, and the equivalent contact area A_c is the cross-sectional area of the smaller particles.

The formula for calculating the contact force between particles is as follows:

$$\begin{aligned} F_n(t+\Delta t) &= F_n(t) - K_n \Delta u_n \\ F_s(t+\Delta t) &= F_s(t) - K_s \Delta u_s \end{aligned} \tag{3}$$

where Δu_n and Δu_s are the normal displacement increment and tangential displacement increment between the contact particles, respectively.

The formula for calculating the moment between particles is as follows:

$$\begin{aligned} M_n(t+\Delta t) &= M_n(t) - K_s J \Delta\theta_n / A_c \\ M_s(t+\Delta t) &= M_s(t) - K_n I \Delta\theta_s / A_c \end{aligned} \tag{4}$$

where M_n and M_s are the torque and bending moment between particles, respectively; I and J are the moment of inertia and polar moment of inertia between contact particles, respectively; and $\Delta\theta_n$ and $\Delta\theta_s$ are the incremental difference in the twist and bending angle between the particles, respectively.

$$\begin{aligned} J &= \pi(R_1 + R_2)^4/32 \\ I &= J/2 \\ A_c &= min(2R_1, 2R_2) \\ K_n &= \bar{E}A_c/(R_1 + R_2) \\ K_s &= \bar{G}A_c/(R_1 + R_2) \end{aligned}$$

where R_1 and R_2 are the contact particle radius; K_n and K_s are the normal and tangential stiffnesses of the contact particles, respectively; and $\bar{E}$ and $\bar{G}$ are the average elastic modulus and shear modulus, respectively.

According to the Mohr-Coulomb criterion and maximum tensile stress criterion, the contact forces of equations (3) and (4) are modified (Normal force is positive with pressure).

If $-F_n \geq TA_c$, then $F_n = F_s = 0$, $T = C = 0$;

if $F_s \geq F_n \tan(\varphi) + CA_c$, then $F_s = F_n \tan(\varphi)$, $T = C = 0$; and

if any of the inequalities in (5) are satisfied, the contact between particles will no longer transmit the moment.

$$\left(\frac{-F_n}{A_c} + \frac{M_s}{I}R_{ave}\right) \geq T \text{ or } \left(\frac{|F_s|}{A_c} + \frac{M_n}{I}R_{ave}\right) \geq (\sigma \tan(\varphi) + C) \tag{5}$$

where $R_{ave} = (R_1 + R_2)/2$, T, C and φ are the tensile strength, cohesion

and internal friction angle, respectively.

In the 2D numerical calculation, the essence of the contact between the block and particle elements is judgment of the relative position between the particle center and block edge. The creation of the contact between the particle and block needs to satisfy both of the following:

1 The distance between the particle center and block edge is less than or equal to the radius of the particle: $d = |V_{kl} \cdot n| \leq R$
2 The projection point of the particle center on the boundary edge of the block is located inside the body edge of the block:

$$d_{lp} \leq d_{lm},\ d_{mp} \leq d_{lm}$$

where l and m are the two endpoints of the block edge, V_{kl} is the relative position vector for the particle center k to the endpoint l, p is the projection point of the particle center on the boundary edge of the block, n is the unit normal vector of the block edge, d_{lm} is the distance between point l and point m, d_{lp} is the distance between point l and point p, and d_{mp} is the distance between point m and point p.

Once the particles have established a contact relationship with the block element boundary, contacting normal and tangential springs will be automatically created. The interpolation coefficient of contact point p between the block and particle will be automatically determined through the following formula:

$$\omega_l = d_{mp}/d_{lm},\ \omega_n = d_{lp}/d_{lm}$$

where ω_l and ω_m are the interpolation coefficient of point p to point l and the interpolation coefficient of point p to point m.

In order to verify the correctness and accuracy of the coupled approach, the simulation of the Brazilian test of phyllite specimen is carried out by referring to the literature.[29] The phyllite specimen is simulated by particle element method, the numerical model of isotropic Brazilian disk is generated as shown in Fig. 2a, the diameter of the particles is 0.4 mm, and the space between foliations is 5 mm. The bearing plate is simulated by block element method, the loading velocity of top bearing plate is 1 nm/step, and the bottom nodes of another bearing plate are fixed. The numerical parameters are obtained from the laboratory testing of the horizontal and vertical foliation specimens, as shown in Table 1. The simulation results are compared with the numerical and experimental results from the literature, as shown in Figs. 2 and 3.

It can be seen from Fig. 2b, c and d that the phyllite fracture patterns of the simulation are in good agreement with numerical simulation and laboratory tests in the literature. Moreover, as indicated in Fig. 3, good agreement in the values of failure strength is found between the numerical and experimental results. Therefore, the coupled approach of particle element and block element is suitable for simulating the fracture process of the material from the continuous state to the discontinuous state.

2.2. Support model and numerical constitutive

To realistically simulate the top-coal caving process, the coupled method of particle and block elements from section 2.1 is used to simulate the interaction between the rock particles and hydraulic support. Moreover, the constitutive model of hydraulic support is introduced into the CDEM, which can simulate the variation regularity of the support working resistance during the coal drawing process.

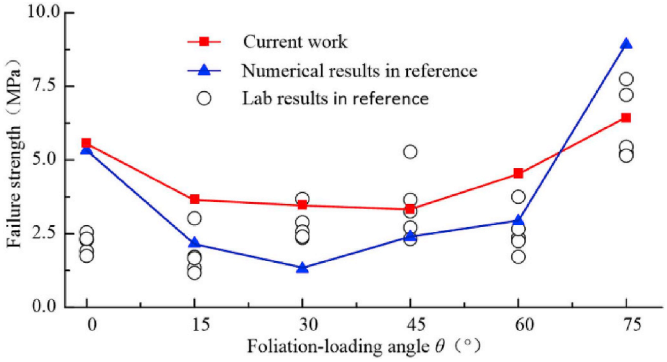

Fig. 3. Failure strength of simulation in comparison with the reference.

As shown in Fig. 4a, the contact element is introduced into the support model. The blue contact elements are used to simulate the contact between inner and outer columns. The inner column is subjected to the normal constraint of the outer column, and thus, the normal stiffness of the contact element should be considered a penalty stiffness, which is as large as possible. The tangential stiffness of the contact element is taken as 0 because the inner column can move freely along the axis inside the outer column. Meanwhile, red contact elements of Fig. 4a are used to simulate variation regularity of the support working resistance by introducing the constitutive model of support in Fig. 4b. As indicated in Fig. 4b, as the working resistance is in the range of P_1 to P_2, which is determined by the product of hydraulic stiffness and axial downward displacement of the inner column. When the working resistance is greater than P_2, which is set as P_2 to simulate the adjustment of the working resistance after the relief valve of hydraulic support is opened.

2.3. The theoretical model of top-coal drawing

Top-coal is crushed into fragments under overburden pressure, which is drawn out through a drawing opening at the rear of the hydraulic support. However, the process of coal drawing on the cross-section parallel to the coal face is not affected by the support structure. Therefore, the top-coal drawing theory for a single drawing opening on the cross-section parallel to the coal face can be referred to as the Bergmark–Roos theory.[30–32]

The main hypothesis employed in the Bergmark–Roos model is that fragments move in straight lines from their resting points to the drawing opening where they are continuously removed; fragments are influenced solely by gravity and frictional forces; and the acceleration of a single fragment is constant during the moving process. The schema of the Bergmark–Roos model is indicated in Fig. 5.

The boundary equation of the top-coal drawn in the polar coordinates system:

$$r_0 = (r_{max} - r_1)\frac{\cos\theta - \cos\theta_G}{1 - \cos\theta_G} + r_2 \tag{6}$$

Based on Fig. 5, the distance from the coordinate origin to any point on the drawing opening is as follows:

$$r_2 = \frac{r_1}{\cos\theta} = \frac{D}{2\tan\theta_G \cos\theta} \tag{7}$$

Table 1
The numerical parameters in the simulation of Brazilian test.

	Density (kg/m^3)	Elastic modulus (Pa)	Poisson's ratio	Tensile strength (Pa)	Cohesion (Pa)	Internal friction (°)
Bearing plate	7850	2.0E+11	0.25	/	/	/
Rock matrix	2800	3.0E+10	0.25	11.89E+06	11.89E+06	26
Foliation	2519	2.4E+10	0.25	2.16E+06	2.16E+06	26

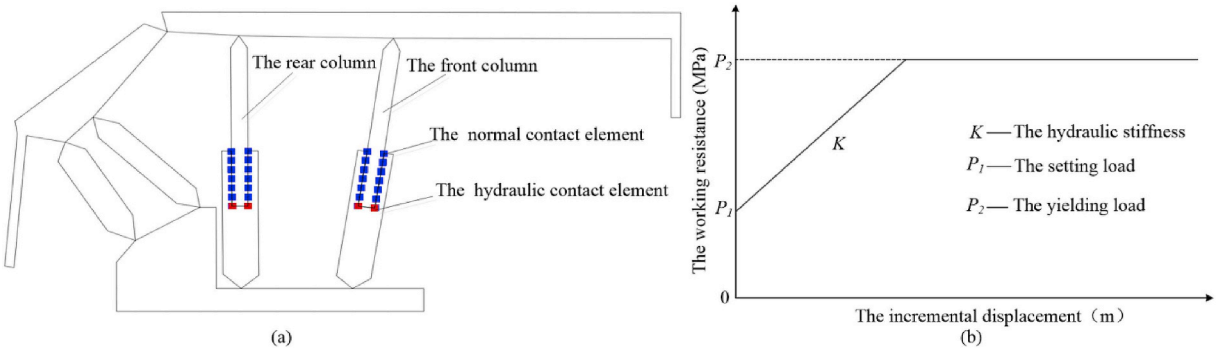

Fig. 4. The support numerical models: (a) the distribution of contact elements in the support model and (b) numerical constitutive model of support.

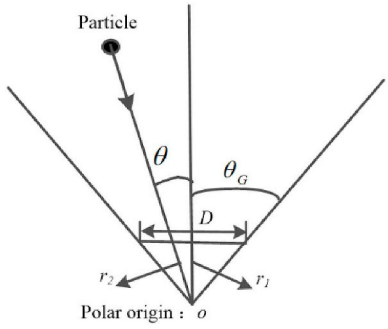

Fig. 5. The schema of the Bergmark–Roos model.

where

$$r_1 = \frac{D}{2\tan\theta_G} \tag{8}$$

Substituting Equations (7) and (8) into Equation (6), we obtain the following:

$$r_0 = \left(r_{max} - \frac{D}{2\tan\theta_G}\right)\frac{\cos\theta - \cos\theta_G}{1-\cos\theta_G} + \frac{D}{2\tan\theta_G\cos\theta} \tag{9}$$

where r_1 is the distance from the center of the drawing opening to the polar origin, m; r_2 is the distance from any point on the drawing opening to polar origin, m; θ is the angular coordinate of the particles; θ_G is the maximum allowed angle for displacement, the angle at which the friction force equals the particle weight; r_{max} is the largest distance from the polar origin to the drawing body boundary, m, which occurs at $\theta = 0$; and D is the drawing opening size, m.

3. Simulation of the top-coal caving process

3.1. Numerical model and parameters

In this study, the panel 8202 of Tongxin Coal Mine is an engineering background. The depth of coal seam is 377 m to 517m, the average thickness of coal seam is about 15 m, the length of working face is 200 m, the working face advance length is 2184.5 m, and the service life of panel is 21.1 months. Because the automated top-coal caving in extra-thick coal seams is a complex three-dimensional space and time evolution process including coal extraction and overburden caving, it will be a huge and complex task to study the automated top-coal caving of panel 8202 by 3D numerical model. This paper decomposes the complex process of automated top-coal caving into two directions, the cross-sections parallel and perpendicular to the coal face, respectively.[20,33] Moreover, the mechanism of top-coal caving in three-dimensional space is obtained by comparing and analyzing the mechanism of top-coal caving in two directions. Based on this, the simulation of automated top-coal caving under the cooperation of 100 coal drawing openings is carried out to optimize the automated top-coal caving technology.

For the automated top-coal caving research, the support force in the caving process is the major focus to ensure the safety of the top-coal caving process.[19,34] In the advance direction of the working face, the top-coal is broken and drawn out under the interaction between hydraulic support and surrounding rocks. Therefore, as shown in Fig. 6a and Fig. 6b, the coal-rock strata and support models are established to study the mechanism of top-coal caving. As indicated in Fig. 6a, the coal-rock strata model in the face advance direction is established according to the drilling histogram of panel 8202 in Tongxin Coal Mine. The average thickness of 3–5 # coal is about 15 m (Groups 1–4), above the coal seam, which is followed by 4.5-m-thick carbon mudstone (Group 5), 1.33-m-thick carbon mudstone (Group 6), 2.54-m-thick 2# coal (Group 7), 3.84-m-thick sandy mudstone (Group 8), 0.84-m-thick 1# coal (Group 9), 5.13-m-thick sandy mudstone (Group 10), 4.38-m-thick coarse sandstone (Group 11), 2.85-m-thick fine sandstone (Group 12) and 5.01-m-thick coarse sandstone (Group 13). As shown in Fig. 6b, the models of hydraulic support and armored face conveyer in the face advance direction are also established based on the actual conditions of the panel. The block element method of section 2.1 is used to simulate the far-field load rock strata and hydraulic support. The rigid wall is used to equivalently simulate the scraper conveyer. The particle element method with an initial strength discussed in section 2.1 is adopted to simulate the coal and rock layer structure in a potentially broken area. At the same time, in order to draw out the more coal resources as easily and conveniently as possible, the process of top-coal drawing with multi-support cooperation is also the major focus of automated top-coal caving research. The average thickness of 3–5 # coal is 15 m and the cutting height is approximately 4 m, so the caving height of top-coal is 11 m. In the direction of working face, the top-coal has been broken and accumulated above the coal drawing openings. Therefore, a coal-rock model is established, as shown in Fig. 6c, the particle element without strength is used to study the coal-drawing mechanism of single drawing opening, based on this, the simulation of automated top-coal drawing with multi-support cooperation is carried out.

No complete theory can predict macroscopic behavior based on microscopic properties and geometry. The numerical parameters are obtained by inversion, and the coal-rock mechanical properties in the elastic analysis stage are shown in Table 2. The time-step is assumed to be 0.0001 s in the simulation of coal drawing. Since the simulation of the top-coal drawing process is a 2D plane analysis, m^2 is used in this paper as a statistical unit for the coal drawing amount.

3.2. The top-coal caving process of the cross-sections perpendicular to the coal face

In the field, the advance length without coal drawing is 16.2 m after the initial mining of a panel. To draw out top-coal as soon as possible, the blasting pre-cracking in the open-off cut is used to accelerate top-

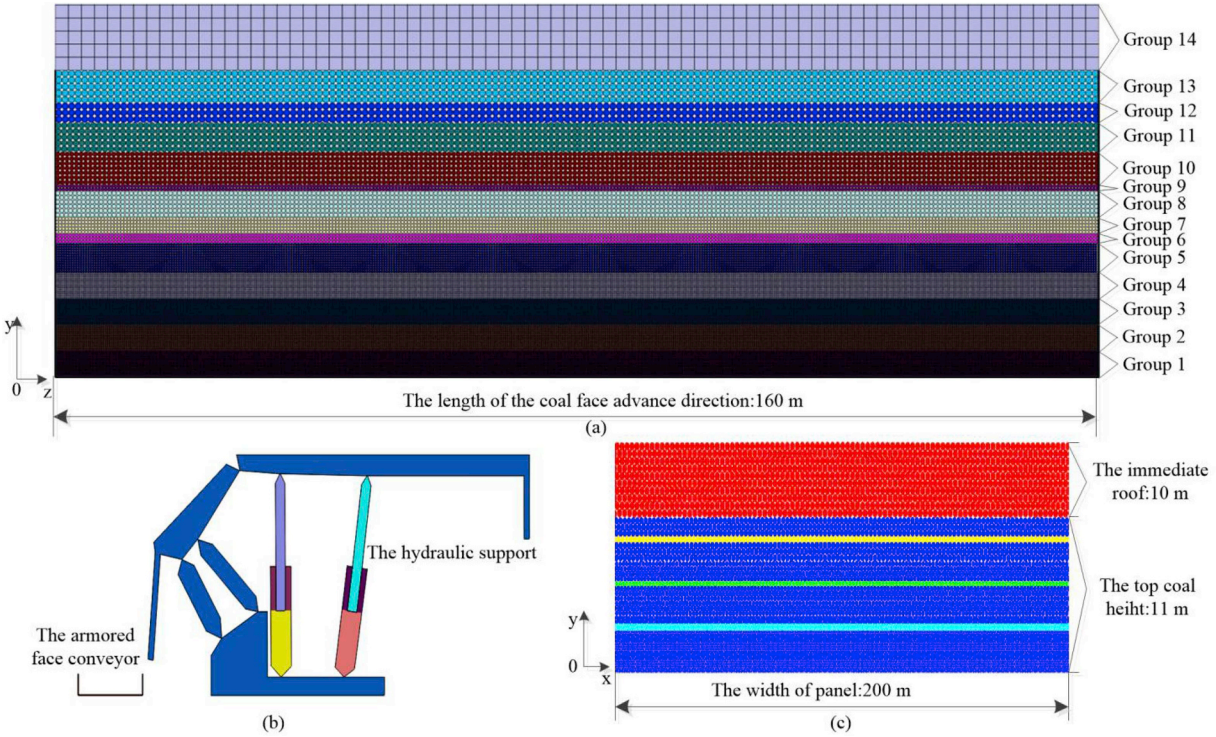

Fig. 6. Numerical models of the panel: (a) the coal and rock model perpendicular to the coal face; (b) armored face conveyer and hydraulic support model; and (c) coal and rock model on the cross-section parallel to the coal face.

coal crushing. The coal drawing termination condition is "rocks appear, close the opening", and the mining process is simulated by deleting 4-m-thick particles from the bottom coal seam. Within 5 m of the open-off cut, the strength parameters of the top-coal and immediate roof are taken as 0 to achieve the blasting pre-cracking effect of the top-coal. After 5 m, because of the influence of the initial cracks and mining disturbances, the strength parameters of the coal-rock mass near the coal face are reduced to a quarter of the elastic parameters. The coal-rock layer structure of the panel before mining is shown in Fig. 7a. As indicated in Fig. 7b, the simulation conducts 50,000 steps after the coal face is advanced from 0 m to 5 m. As indicated in Fig. 7c, the simulation conducts 50,000 steps after the coal face is advanced from 5 m to 10 m. According to Fig. 7d, the simulation conducts 50,000 steps after the coal face is advanced from 10 m to 16.2 m. As indicated in Fig. 7e, hydraulic support is moved into the model after coal face is advanced from 16.2 m to 23.4 m, and the simulation conducts 10,000 steps under the interaction between the hydraulic support and surrounding rocks. Subsequently, the top-coal drawing process simulation begins. Meanwhile, the transport process of the scraper conveyer is simulated by deleting the top-coal particles entering into the range of the rigid wall. When the rock particles begin to enter into the rigid wall after 413543 steps, the process of coal drawing is terminated. The coal-rock layer structure of the panel after the first coal drawing is shown Fig. 7f.

As indicated in Fig. 7e and f, the top-coal is crushed and accumulated behind the support before the initial top-coal drawing, and it is subjected to the gravity of the large rock mass of the immediate roof. However, the top-coal above the canopy of the hydraulic support is in a relatively intact state. The rock mass of the immediate roof and top-coal above the canopy are continuously broken during the coal drawing process. Finally, most of the top-coal above the drawing opening is drawn out under the coal and rock mass gravities.

The drawing body is the status of the drawn top-coal resting above the drawing opening, which represents the range of the drawn top-coal and affects the amount of coal drawing. To study the changing characteristics of the drawing body in the face advancing direction, the drawn particles are marked in the model shown in Fig. 7e to invert the shape of the drawing body during different stages. The inversion results are indicated in Fig. 8.

Table 2
The coal and rock mechanical properties in the elastic numerical analysis stage.

Group	Rock mass	Thickness(m)	Density (kg/m^3)	Elastic modulus (Pa)	Poisson's ratio	Tensile strength (Pa)	Cohesion (Pa)	Internal friction (°)
Group 13	coarse sandstone	5	2519	5.80E+08	0.204	9.54E+06	8.76E+06	34.66
Group 12	fine sandstone	3	2542	6.70E+08	0.276	7.34E+06	9.45E+06	32.81
Group 11	coarse sandstone	4.5	2519	12.0E+08	0.204	9.54E+06	8.76E+06	34.66
Group 10	carbon mudstone	5	2500	9.90E+08	0.2124	2.75E+06	3.68E+06	36.4
Group 9	1 # coal	1	1373	6.20E+08	0.348	3.82E+06	2.40E+06	44.82
Group 8	sandy mudstone	4	2500	9.30E+08	0.1884	4.40E+06	3.30E+06	36
Group 7	2 # coal	2.5	1373	6.20E+08	0.348	3.82E+06	2.40E+06	44.82
Group 6	carbon mudstone	1.5	2340	9.30E+08	0.1884	4.40E+06	3.30E+06	36
Group 5	carbon mudstone	4.5	2340	9.30E+08	0.1884	4.40E+06	3.30E+06	36
Group 4	3-5 # coal	4	1373	6.20E+08	0.348	3.18E+06	2.00E+06	44.82
Group 3	3-5 # coal	4	1373	6.20E+08	0.348	3.18E+06	2.00E+06	44.82
Group 2	3-5 # coal	4	1373	6.20E+08	0.348	2.54E+06	1.60E+06	44.82
Group 1	3-5 # coal	4	1373	6.20E+08	0.348	3.18E+06	2.00E+06	44.82

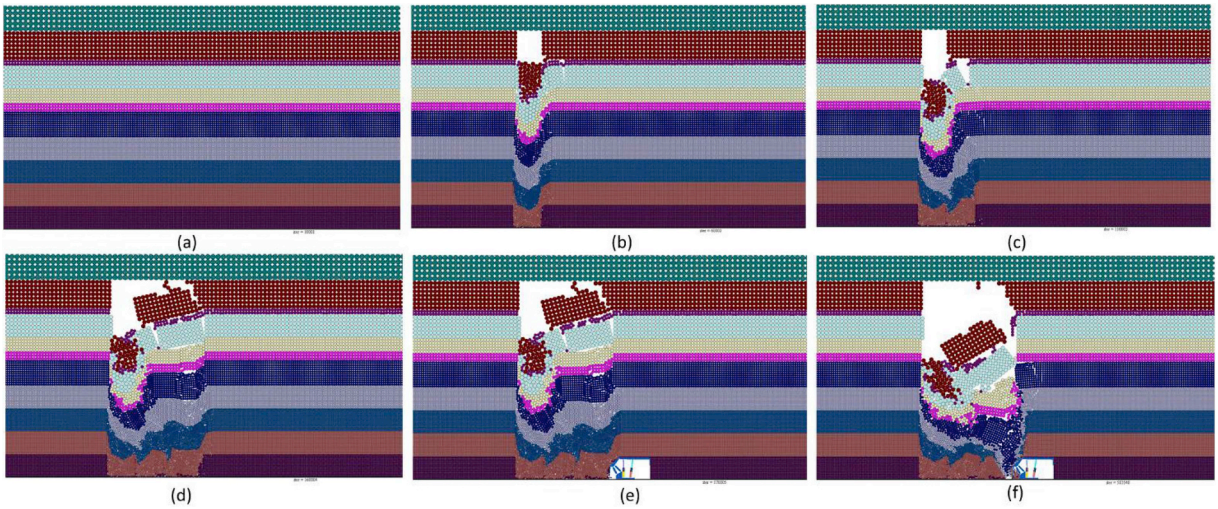

Fig. 7. The coal-rock structure with different coal face advancing lengths: (a) L = 0 m; (b) L = 5 m; (c) L = 10 m; (d) L = 16.2 m; (e) L = 23.4 m, before initial top-coal drawing; and (f) L = 23.4 m, after initial top-coal drawing.

As shown in Fig. 8, the drawing body shape resembles an incomplete ellipsoid, which is cut by the tail beam of hydraulic support during the initial period of the coal drawing process. Due to the impact of the intact top-coal above the support, the shape of the drawing body gradually tilts toward the gob when the coal drawing process proceeds. Eventually, in the coal wall side, the drawing body is bounded by the hydraulic support and intact top-coal; the top boundary of the drawing body presents a flat shape due to the influence of the large rock mass of the immediate roof; in the gob side, the drawing body tilts toward the gob. Overall, the drawing body shape for an extra-thick coal seam presents an irregular shape of a deflected ellipsoid in the face advancing direction.

References[35–41] indicate that after the coal seam is mined, the mining disturbance will cause the surface subsidence. After the surface subsidence occurs, there will be a period of consolidation in the overburden. The subsidence and consolidation of roof strata will affect the hydraulic support load and the caving of coal-rock masses.[19,34] Because this section is studying the top-coal caving mechanism of the initial mining stage, there is no instability failure of main roof strata. As to the effect of subsidence and consolidation on the support load and top-coal caving, the subsidence of main roof strata is distinct than the surface subsidence in the initial mining stage. Therefore, the subsidence of main roof strata is monitored and analyzed to study the top-coal caving and drawing. In the study, the top-coal is not drawn out before the advance length reaches 23.4 m, and the mining process is divided into the four stages as shown in Fig. 7b–e. The subsidence of main roof strata at the end of each stage is monitored, and the subsidence curves are shown in Fig. 9a. After the coal drawing begins, in order to study the effect of subsidence on the top-coal caving and drawing process, the particle of main roof strata with the initial largest vertical displacement is monitored. In the first top-coal drawing process, the vertical displacement curve of the monitored particle is shown in Fig. 9b.

When the coal face advance length increases, the overall subsidence of main roof strata increases as indicated in Fig. 9a. The subsidence of the coal face advance length from 10 m to 16.2 m is significantly larger than the subsidence of the coal face advance length from 5 m to 10 m. Combined with the coal-rock structures of Fig. 7b–d, it can be seen that there is the severe destruction of immediate roof strata when the coal face advances from 10 m to 16.2 m. Meanwhile, it can also be found from Fig. 9a that there is little change in the subsidence of main roof strata when the coal face advances from 16.2 m to 23.4 m. That is because the hydraulic support is timely used to support the top-coal after the bottom coal is excavated, there is basically no further destruction in the top-coal and immediate roof strata as shown in Fig. 7d and e.

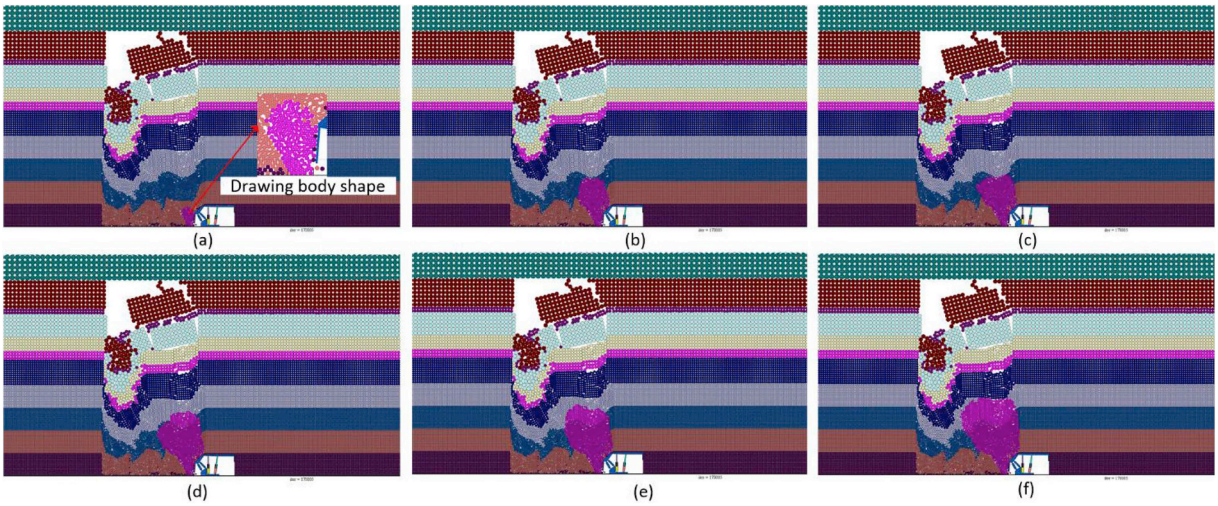

Fig. 8. The drawing body shape at different coal drawing steps: (a) t = 30000 steps; (b) t = 150000 steps; (c) t = 190000 steps; (a) d = 270000 steps; (e) t = 310000 steps; and (f) t = 413543 steps.

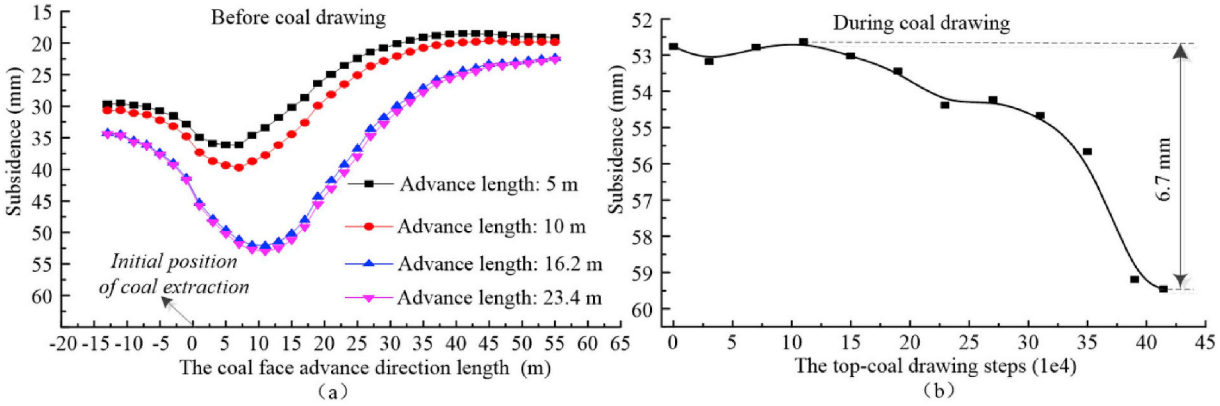

Fig. 9. The subsidence curves of the main roof strata in different mining stages: (a) before the top-coal drawing and (b) during the top-coal drawing.

Because the coal face advance length has reached to 23.4 m before coal drawing, the max subsidence amount of main roof strata reaches 52.76 mm due to the effect of coal extraction, as shown in Fig. 9b. In the first top-coal drawing process, the simulation conducts 413543 steps, and the max subsidence amount of main roof strata is 6.7 mm. The total subsidence amount of main roof strata is 59.46 mm after coal drawing, which is not enough to cause the instability of main roof strata. So that the main roof bears the weight of the overlying strata and the hydraulic support works safely under lower stress states. The top-coal is caved and drawn out under the interaction between hydraulic support, top-coal and immediate roof masses.

The top-coal is drawn out under the interaction between the hydraulic support and surrounding rocks, and the support working resistance can impact the crushing result of the top-coal. Therefore, the study on variation regularity of support working resistance is important for top-coal drawing. Because the strength parameters of the coal-rock mass near the coal face are reduced to a quarter of the elastic parameters, the setting load (P_1) of the front and rear columns in the support constitutive model from section 2.2 are considered 0 to avoid having a large dynamic impact and ensuring the stability of the particle model. The working resistance curves of the hydraulic support front and rear columns during the simulation process of coal drawing are shown in Fig. 10.

As indicated in Fig. 10, the working resistances of the front and rear columns increases along with the coal drawing process, which reach the peak value after 18000 steps. The front column is subjected to a larger pressure transmitted by the coal-rock mass and the working resistance increases to approximately 30 MPa. Then, the working resistance undergoes minor changes as the coal drawing process continues. However, the rear column is subjected to less pressure and the working resistance only increases to approximately 8 MPa, which is because the partial top coal above the hydraulic support canopy is crushed and drawn out. As the coal drawing process proceeds, the working resistance gradually decreases because the crushed top coal above the rear column is continuously drawn out.

The movement of overburden strata in ordinary mining stages can induce vast strata pressure and result the cracking, dislocating and flowing of top-coal. The top-coal drawing characteristics during ordinary mining stages are the general and important, which is necessary to be investigated. Therefore, after the initial top-coal drawing, another 24 cycles of coal drawing simulation are carried out, and the distance of every support advance cycle is 0.8 m. Based on this, the relationships of the coal drawing amount, coal drawing steps, support resistance and coal-rock structure are analyzed.

With increasing support moving, the coal drawing amounts and coal drawing simulation iteration steps are counted in sequence before the support is advanced. As shown in Fig. 11, the variation of coal drawing amount and coal drawing steps shows the basically consistent trend with increasing support moving. The initial coal drawing amount and coal drawing steps respectively reach 76.4 m^2 and 414395 steps, which is significantly larger than the values of subsequent coal drawing cycles. Due to the continuity of the coal drawing process, the initial coal drawing will affect subsequent coal drawing cycles, the coal drawing amount and coal drawing steps remain relatively low values until the 6th support moving. From the 6th to 25th support moving, the coal drawing amount and coal drawing steps are in normal periodic fluctuation. In general, the coal drawing amounts of adjacent coal drawing cycles influence each other, the previous higher drawing amount can lead to a lower drawing amount in the subsequent coal drawing cycles and vice versa.

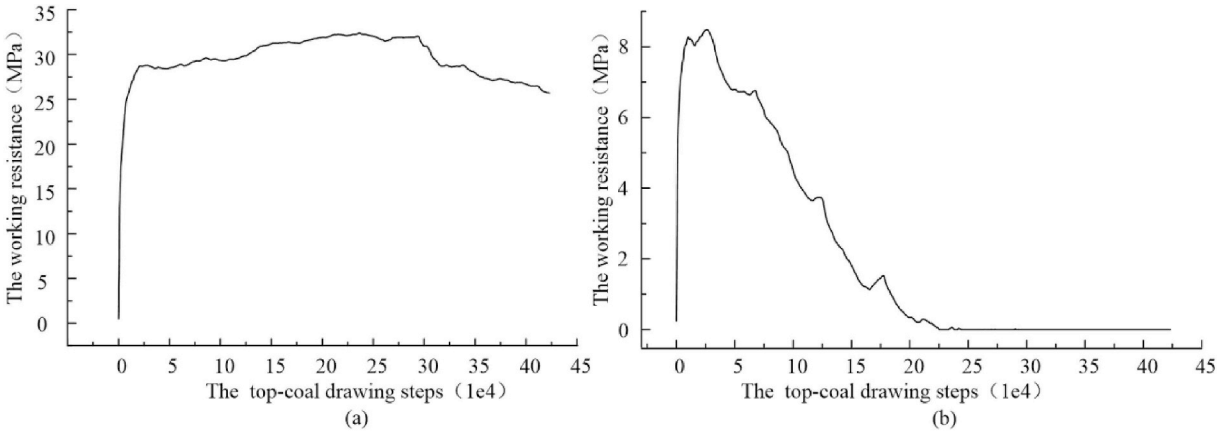

Fig. 10. The working resistance curves of the support: (a) working resistance of the front column and (b) working resistance of the rear column.

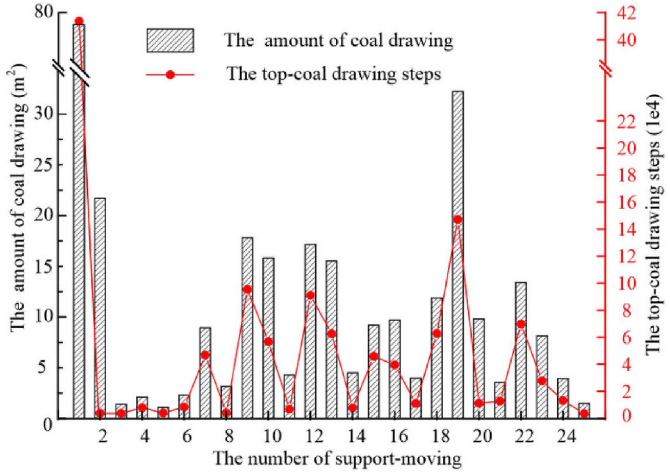

Fig. 11. The coal drawing amount and coal drawing steps with different support-moving numbers.

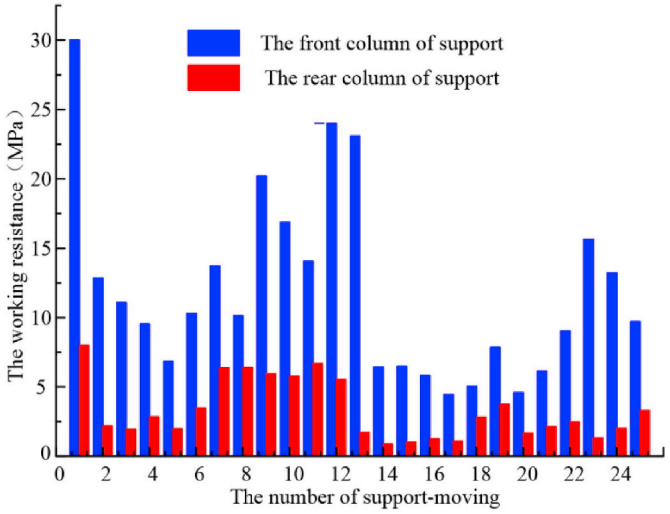

Fig. 12. The support working resistances with different support-moving numbers.

In different coal drawing cycles, the working resistances of the hydraulic support front and rear columns are monitored. The working resistance peaks are counted in Fig. 12. It can be seen that the working resistance peaks under different coal drawing cycles indicate the periodic variation. The working resistance peaks of the front column are larger than the rear column, and the working resistance fluctuation is greater than the rear column.

In order to investigate the variation mechanism of coal drawing amount and support resistance, the coal-rock structures under different support-moving numbers are analyzed in Fig. 13. In general, the coal-rock masses are cracking, dislocating and flowing under the interaction between hydraulic support and surrounding rocks. Subsequently, the top-coal is drawn out by the drawing opening of hydraulic support. From Fig. 13a and b, the coal drawing processes from the 2nd to 6th support moving are affected by the large gangue hopper formed in the initial coal drawing process, therefore, the coal drawing amounts until 6th coal drawing cycle are smaller. As shown in Fig. 13c, after the 12th coal drawing cycles terminated, the immediate roof above the support canopy fractures, which may lead the larger working resistance peak of front column. It can be seen from Fig. 13d that the top-coal above support canopy is relatively fragmentized, so the working resistance peaks of front and rear columns are lower in some coal drawing cycles near the 15th support-moving. From Fig. 13e, the large rock blocks of immediate roof are located above the coal drawing opening, moreover, the blocks are in moving state. Due to the gravity of large rock blocks, the coal drawing amount in the 19th coal drawing cycle is larger. As shown in Fig. 13f, most of the broken coal-rock blocks are located in goaf, the hydraulic support bears the weight of intact coal-rock masses, so the working resistance peak of the front column is larger in the 23rd coal drawing cycles.

3.3. The top-coal drawing process of the cross-sections parallel to the coal face

The drawing body shape on the cross-section parallel to the coal face is not affected by the hydraulic support structure during the coal drawing process. Therefore, the numerical model without support is used to study top-coal drawing, as indicated in Fig. 6c. Because the drawing opening width of the support on the cross-section parallel to the coal face is 1.75 m, a layer of particles within the width range of 1.75 m in the middle of the model bottom boundary are deleted to simulate the top-coal caving process of a single drawing opening. Before the top-coal is drawn out, the top-coal is broken into fragments during mining and resistance generated by movement between fragments. Therefore, the strength parameters of the top-coal in the simulation are set to 0. The coal drawing termination condition is “rocks appear, close the opening”.

As shown in Fig. 14, after the top-coal is drawn out, the interface of coal and rock shows a hopper shape for a single drawing opening. In order to study the drawing body shape and the movement trajectory of the top-coal, the particle marking method is applied. The specific details are as follows: after the top-coal is drawn out, the ID numbers of all the released particles are counted, and then all the particles with the same ID number are marked in the numerical model before coal drawing. As shown in Fig. 15, the drawing body shape of top-coal is obtained, which is an approximate ellipsoidal shape on the cross-sections parallel to the coal face.

The typical particles in the ellipsoid boundary of Fig. 15 are marked to track the movement trajectory of the top-coal during coal drawing. At different coal drawing steps, the location of marked particles in broken top-coal is shown in Fig. 16, and the overall migration trajectory of all marked particles in the whole drawing process is shown in Fig. 17a.

Equation (9) of section 2.3 is the boundary equation of the drawing body theory model. In this section, r_1 is considered to be the thickness of the top-coal (11 m); $\theta_G = 30^\circ$, D is considered to be the width of the support (1.75 m), and Equation (9) is simplified to Equation (10).

$$r_0 = \frac{11(2\cos\theta - \sqrt{3})}{2 - \sqrt{3}} + \frac{7\sqrt{3}}{8\cos\theta} \tag{10}$$

According to Equation (10), the theoretical model of the top-coal drawing body shape on the cross-section parallel to the coal face is indicated in Fig. 17b.

As shown in Fig. 16, the marked particles at different coal drawing steps still exhibit an approximate ellipsoid shape in spatial position, and the top-coal in this ellipsoid can be finally drawn out by the drawing opening. Moreover, the partial top-coal particles outside the ellipsoid boundary are loose but not drawn out. As indicated in Fig. 17a, because of the collision and jamming effect of top-coal particles in the top-coal drawing process, the marked particles do not move strictly along the straight lines from the top-coal ellipsoid boundary to the drawing opening, however, the migration trajectory is in basically accordance with the theoretical model of Fig. 17b. Therefore, a conclusion can be obtained through the comparison of Figs. 15, Figs. 16 and 17 that on the cross-section parallel to the coal face, the simulation of coal drawing for single support is in accordance with the theoretical model.

The drawing speed of the top-coal affects the coal drawing time and then affects the coal transportation of the scraper conveyer and the

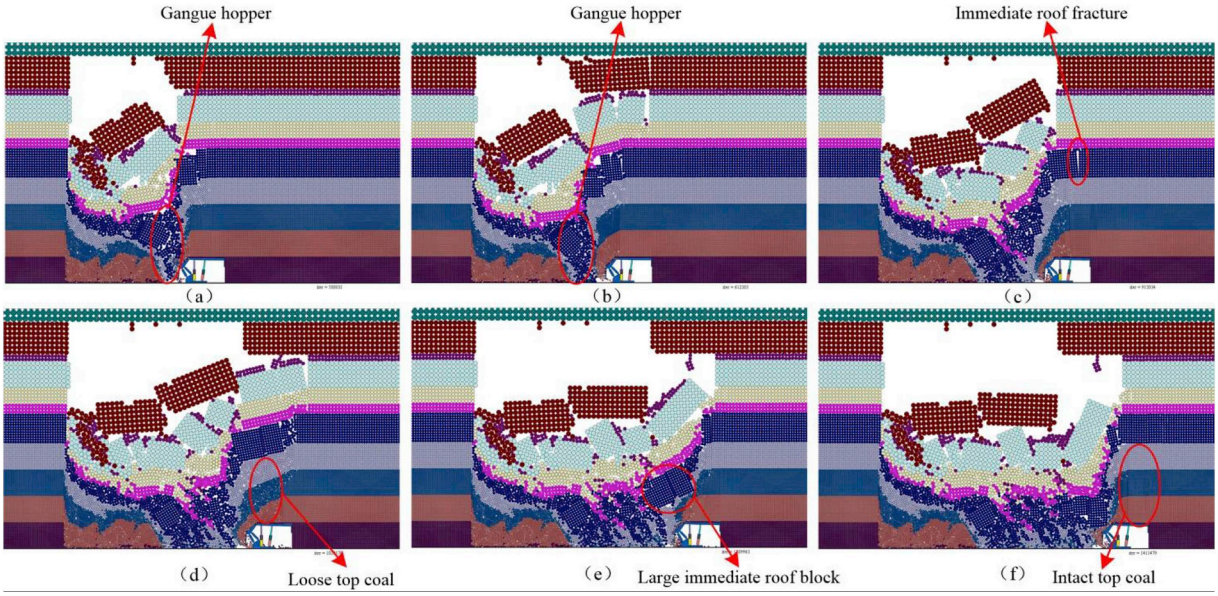

Fig. 13. The coal-rock structure with different support-moving numbers: (a) the 2nd support-moving; (b) the 6th support-moving; (c) the 12th support-moving; (d) the 15th support-moving; (e) the 19th support-moving; and (f) the 23rd support-moving.

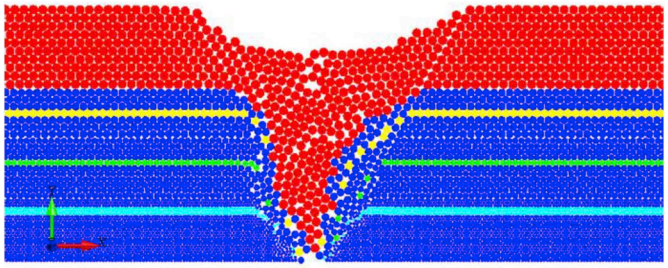

Fig. 14. The coal-rock interface after coal drawing.

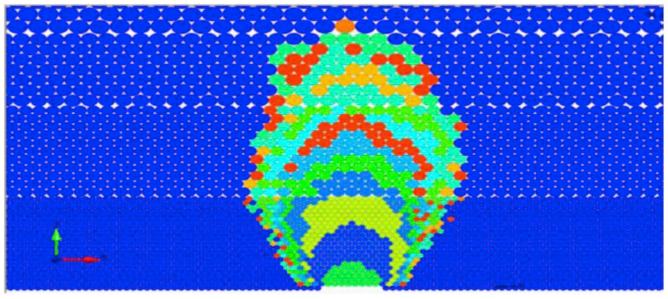

Fig. 15. The shape of the drawing body.

advancing of hydraulic support. As shown in Fig. 18, the drawing speed and horizontal stress of the top-coal fragments near the drawing opening are analyzed to study the variation regularity.

As indicated in Fig. 18, there are two main stages in the coal drawing process, and the horizontal stress and drawing speed of top-coal fragments near the drawing opening both show periodic fluctuations. The curve of the horizontal stress and coal drawing speed changes almost synchronously during the first stage of coal drawing, and thus, the horizontal stress promotes the drawing out of top-coal. The horizontal stress and drawing speed show the opposite change during the second stage, and therefore, the horizontal stress hinders drawing out of the top-coal.

4. Automated top-coal caving techniques

Though the drawing body shape of top-coal is a 3D structure in space, on the cross-section parallel to the coal face, the overall profile shapes of the drawing body above all drawing openings can impact the top-coal recovery rate of the entire working face. The coal drawing theory of a single drawing opening is also applicable to study the coal drawing process for multiple drawing openings based on section 3.3. Therefore, in order to optimize the automated top-coal caving technology, the Bergmark–Roos model for coal drawing of single support is extended into the collaborative coal drawing of multiple supports. First, in this section, the simulation of traditional coal caving and automated one-round coal caving is performed to analyze the advantages of automated coal caving technology. Then, the simulation of different automated coal caving rounds is conducted to optimize the parameters of automated coal caving. Finally, the top-coal drawing results of different technologies are analyzed and discussed. In this section, the coal drawing time of the engineering site is the input parameter of the automated control device, which determines the opening and closing of the drawing opening. Therefore, the coal drawing time is the specify iteration steps of the automated top-coal drawing simulation. Although, the automated coal drawing time of the engineering site is still under study, which is necessary to comprehensively consider the relationship between the field equipment, top coal recovery rate and coal transportation efficiency. However, in the simulation of this section, the total iteration step of the coal drawing for each coal drawing opening is taken as 60000 steps by inversion of simulation, which can draw out most of the top-coal in the working face and achieve better simulation effect of automated coal drawing.

4.1. Comparison of automated and traditional top-coal caving

In the field, the working face width is 200 m and the drawing opening width of the support is 1.75 m. As indicated in Fig. 6c, the 2D model is used to study the overall coal drawing result of 100 supports in a coal cutting cycle. The coal drawing process of 100 drawing openings is simulated from left to right in the model. As indicated in Fig. 19a, the traditional top-coal caving technology adopts “rocks appear, close the opening”, and no rock is mixed into the top-coal drawn out. Therefore, rock particles are deleted to simulate the process of top-coal drawing

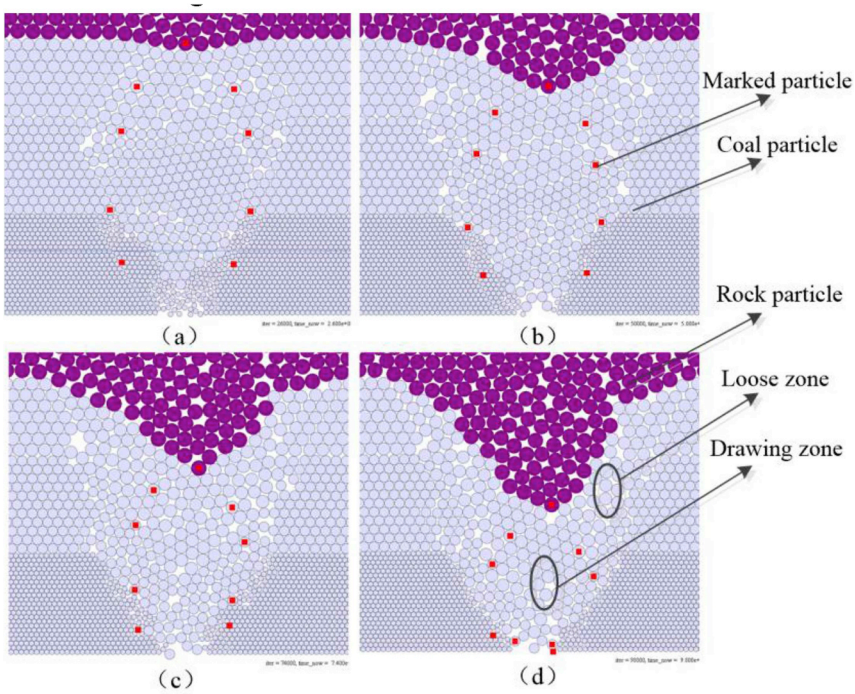

Fig. 16. The location of marked particles in broken top-coal at different coal drawing steps: (a) t = 26000 steps; (b) t = 50000 steps; (c) t = 74000 steps; and (d) d = 98000 steps.

when they enter into the rigid wall of the drawing opening. As shown in Fig. 19b, during the automated coal caving process, rock particles are mixed into the top-coal drawn out because time is a control variable of coal drawing. Therefore, **in order to furtherly** analyze the coal-rock mix and top-coal recovery rates, coal and rock particles are collected through the rigid walls of 100 drawing openings when they are drawn out. As shown in Table 3, the statistical comparison of coal-rock drawing amount from 100 drawing openings is conducted to analyze the results of coal drawing using two technologies.

As indicated in Fig. 19, coal and rock are mixed into each other at the coal-rock interface of the traditional coal caving. Meanwhile, a large amount of rocks are mixed into the top-coal drawn during the automated one-round coal caving. Table 2 shows that the top-coal recovery rate of the automated coal caving is 83.7%, which is higher than the recovery rate (81.6%) of traditional coal caving. However, the rock mixed rate (7.52%) of automated coal caving is also higher than the rock mixed rate (0) of traditional coal caving.

As shown in Fig. 20 and Table 3, the top-coal drawing amount from 100 drawing openings are statistically analyzed to further compare the advantages and disadvantages of the two technologies.

According to Fig. 20 and Table 4, for automated coal caving technology, the top-coal drawing amount average of 100 drawing openings is 16.65 m^2 larger than the coal drawing amount average (15.01 m^2) of traditional coal caving. Moreover, the coal drawing amount standard deviation (1.83 m^2) is less than that in traditional coal caving (8.23 m^2).

Some rocks may be mixed into the top-coal drawn during the automated one-round coal caving process; however, the coal drawing amount average of the automated coal caving is larger, and thus, the top-coal recovery rate is higher than that of traditional coal caving. Because the standard deviation of the coal drawing amount is smaller in automated coal caving, and the top-coal drawing amount of each drawing opening is more uniform than in traditional top-coal caving, the operation of workers is simpler, and the transportation efficiency of the scraper conveyer is greater. Overall, the automated top-coal caving technology is better than the traditional top-coal caving technology.

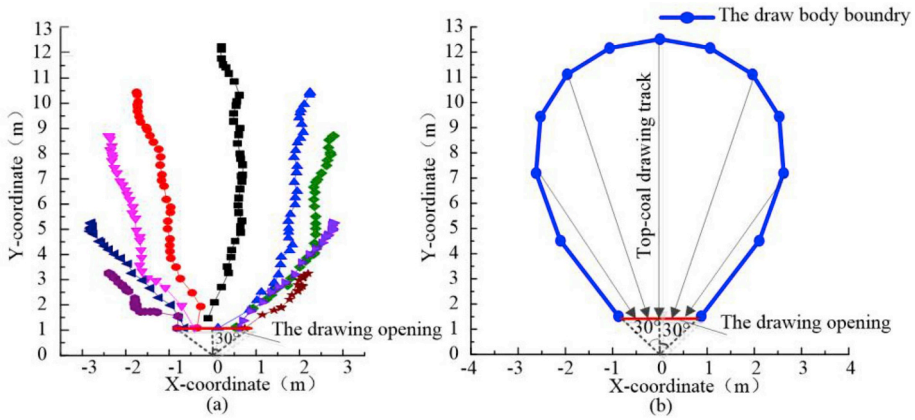

Fig. 17. The trajectory of top-coal moving: (a) the moving trajectory of simulation and (b) theory model.

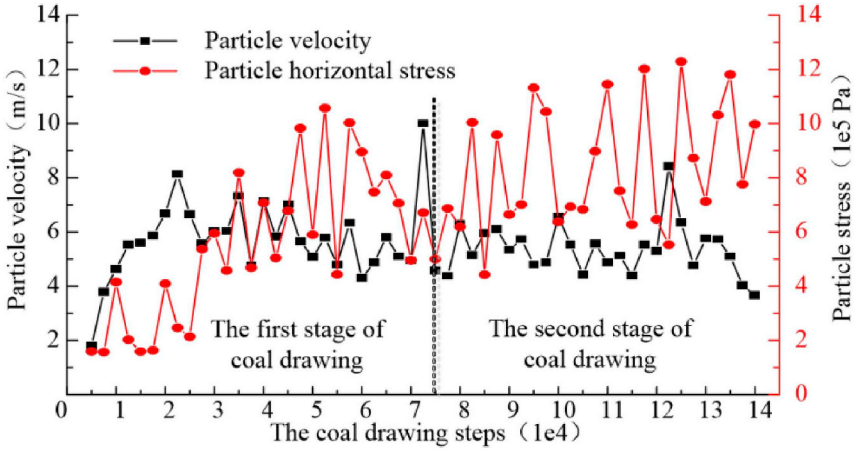

Fig. 18. The drawing velocity and horizontal stress of the top-coal fragments.

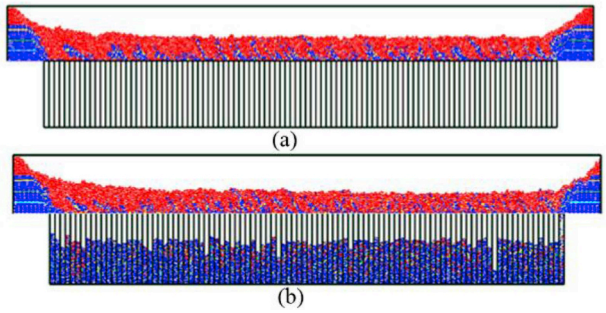

Fig. 19. The results of coal drawing using different technologies: (a) traditional coal caving and (b) automated one-round coal caving.

4.2. The effects of different rounds on automated top-coal caving

To solve the rock mixed rate (7.52%) problem of the automated one-round coal caving in section 4.1, in this section, the impact of different rounds on the automated coal caving process is studied. In the simulation, because the total time of coal drawing is constant, the coal drawing time of each round is negatively correlated with the total rounds of top-coal caving.

Under different rounds of automated coal caving, the coal-rock interface and coal-rock mixing of top-coal drawn out are indicated in Fig. 21.

According to Fig. 21, the coal-rock interface affects the top-coal recovery rate and coal-rock mixing in top-coal caving. The coal-rock interfaces of automated one-round coal caving are mixed with each other, and therefore, large amount of rocks are mixed into the top-coal drawn out. However, the coal-rock interfaces of automated multi-round coal caving show an obvious layered distribution, and therefore, a small amount of rocks are mixed into the top-coal drawn out. Moreover, the more rounds of automatic top-coal caving, the layered distribution of the coal-rock interface is more gradual.

Under different coal drawing rounds for 100 drawing openings, the top-coal recovery and rock mixed rates are statistically analyzed to optimize the total rounds of coal drawing. The results are shown in Table 5.

As shown in Table 5, the automated one-round top-coal caving has the largest top-coal recovery amount; however, 7.52% of the rock mixed rate in the top-coal drawn out is also the largest. The top-coal recovery rate gradually increases as the total rounds of automated top-coal caving increase from 2 to 6. The recovery rate reaches the maximum when the total rounds increase to 4, and then, the recovery rate gradually decreases. As the total rounds increase from 2 to 6, the average recovery rate of top-coal remains at 79.4% and does not increase significantly. Furthermore, the rock mixed rate in the top-coal drawn out is less than 1%.

The statistical analysis of the total top-coal drawing amount for the 100 drawing openings is performed to further study the influence of the total rounds of coal drawing. The result is shown in Fig. 22.

As indicated in Fig. 22, the standard deviation of top-coal drawing amount decreases from 2.21 m^2 to 1.23 m^2 when the total rounds of automated top-coal caving increase from 2 to 6, and thus, the difference in the coal drawing amount for each drawing window shows a decreasing trend. Moreover, the standard deviation change rate of the top-coal drawing amount of four-round coal caving is the largest, and the trend slows as the total rounds increase to more than 4. Meanwhile the coal drawing amount average increases from 14.35 m^2 to 14.88 m^2 when the total rounds increase from 2 to 4. However, the average amount of coal drawing begins to decrease as the total rounds increase from 4 to 6. Therefore, the four-round coal caving is the optimal automated top-coal caving technology considering the rock mixed rate, top-coal recovery rate and standard deviation of coal drawing amount.

4.3. Different top-coal caving technologies

The collaborative coal drawing of all supports determines the final result of coal drawing in working face. Based on section 3.3, the single drawing opening can draw out the top-coal in an ellipsoidal area above the drawing opening, and then, a gangue funnel will be formed. Using traditional coal caving technology, the window of the first drawing coal will draw out the top-coal in a larger ellipsoidal sphere, and then, a larger gangue hopper is formed. Due to the impact of the adjacent drawing opening, the window of subsequently drawing coal can only draw out the top-coal in the range of a smaller ellipsoid to avoid drawing out rocks. Then, a smaller gangue hopper is formed. In the

Table 3
Comparison of top-coal drawing amount in traditional and automated coal caving technologies.

Total coal amount 1839.9 m^2	Top-coal caving technology	Coal drawing amount (m^2)	Rock drawing amount (m^2)	Top-coal recovery rate (%)	Rock mixed rate (%)
Total rock amount 941.6 m^2	Automated coal caving	1538.78	125.1	83.7	7.52
	Traditional coal caving	1500.5	0	81.6	0

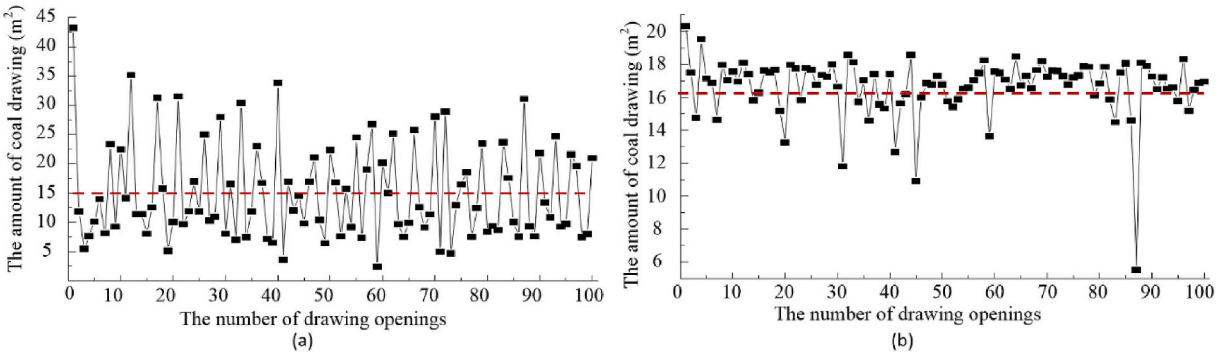

Fig. 20. The coal drawing amount of each drawing opening using different technologies: (a) traditional coal caving and (b) automated one-round coal caving.

Table 4
Statistics of coal drawing amount for each drawing opening in traditional and automated technologies.

Drawing opening number: 100	Automated top-coal caving	Traditional top-coal caving
Coal drawing amount standard deviation (m^2)	1.83	8.23
Coal drawing amount average (m^2)	16.65	15.01

entire working face, each drawing opening only can draw out the top-coal in large and small ellipsoids in sequence, and thus, the difference in the coal drawing amount for each drawing opening is larger. Therefore, workers operation are heavy and complex. Moreover, the transport efficiency of the scraper conveyer is lower.

The coal drawing time is a control variable for the automated top-coal caving, and therefore, the coal drawing operations are simple and orderly. However, for automated one-round coal caving, each drawing opening only performs one-round coal drawing at a constant time, and then, the gangue hoppers are formed. The coal drawing time for the one-round coal caving technique is larger than the coal drawing time of the multi-round coal caving technique, and thus, the adjacent drawing openings fully draw out the top-coal and also release excess rocks.

The increase in the total rounds of automated top-coal caving will reduce the coal drawing time of each round, which is because the total coal drawing time is constant. Therefore, the impact of adjacent drawing openings decreases and the top-coal drawing amount from each drawing opening will be more uniform. Moreover, the drawing body shapes of each round will appear as an overall layered distribution. When the total rounds increase, the coal-rock interface above the drawing openings gradually smooths and the top-coal is easily draw out in layers. Thus, the overall top-coal recovery rate is higher and the rock mixed rate in the top-coal drawn out is lower.

In general, the more rounds of automatic top-coal caving, the better the results of coal drawing. However, the coal drawing time of each round is too short to efficiently destroy the arch structure of the rock particles as the total rounds are more than 4, and therefore, the top-coal recovery rate becomes small. Moreover, the number of openings and closings of the drawing opening becomes large as the total rounds increase, which increases the difficulty of automation. In this study,

Table 5
Comparison of automated coal drawing amount for different total rounds.

	Total coal drawing rounds	Coal drawing amount (m^2)	Rock drawing amount (m^2)	Top-coal recovery rate (%)	Rock mixed rate (%)
Total coal	1	1538.78	125.1	83.7	7.52
amount	2	1426.31	8.2	77.6	0.57
1839.0 m^2	3	1443.67	1.7	78.5	0.12
Total rock	4	1482.81	4.8	80.6	0.32
amount	5	1478.63	1.13	80.4	0.08
941.6 m^2	6	1469.65	1.13	79.9	0.08

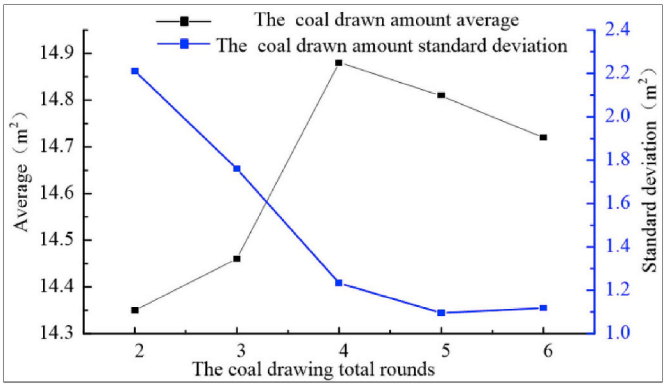

Fig. 22. Statistics of automated top-coal drawing amount for different total rounds.

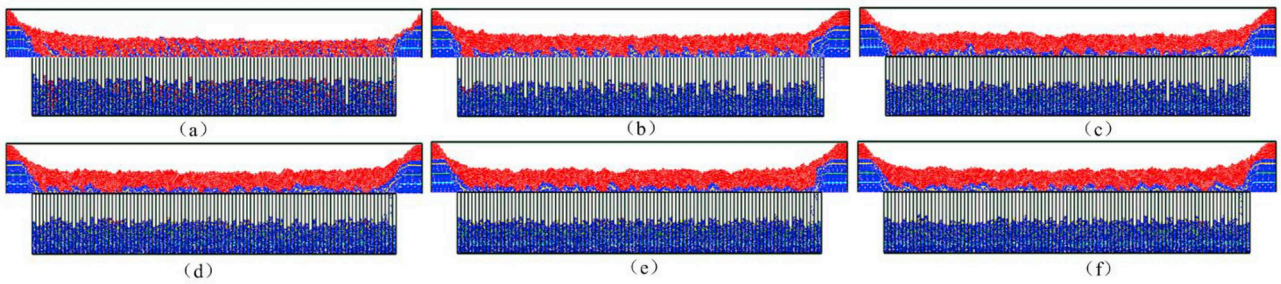

Fig. 21. The results of automated coal caving with different total rounds: (a) n = 1; (b) n = 2; (c) n = 3; (a) n = 4; (e) n = 5; and (f) n = 6.

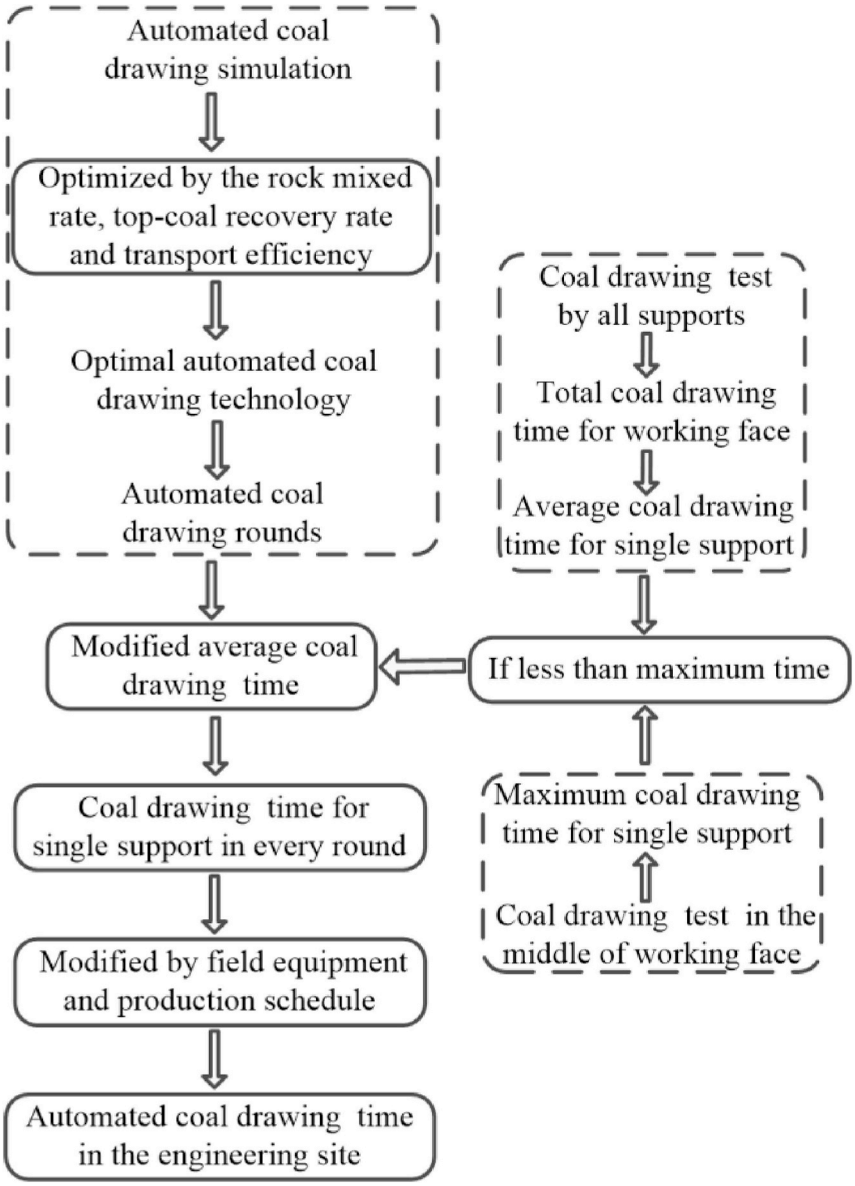

Fig. 23. Flow chart for determining automated coal drawing time.

automated four-round coal caving is the optimal technology; however, the total rounds of automated top-coal caving should be adjusted according to the performance of the automated equipment and specific field conditions.

4.4. Automated coal drawing time

The coal drawing time of the engineering site determines the opening and closing of the drawing opening, which is the important control parameter of the top-coal caving mining. In order to make our research valuable for a practical mining, the correlation between simulation and field coal drawing is analyzed, furthermore, the method of determining automated coal drawing time is discussed.

The coal drawing simulation is terminated after the specify iteration steps, and the total coal drawing steps for each drawing opening is determined by inversion of simulation. The results of Section 4.2 indicate that the simulation under the steps obtained by inversion can achieve better coal drawing effect of entirely working face, which comprehensively considers the movement of coal-rock interface, rock mixed rate, top-coal recovery rate and transport efficiency of the scraper conveyer. Because the shapes of coal-rock blocks in field are different from the particles in simulation, the top-coal drawing time in simulation cannot be directly equal to the coal drawing time in the practical operation. However, the geometric and mechanical boundary conditions of simulation are basically same to the engineering site, so the reasonable automated coal drawing time in field can be determined by the combination of simulation and in-site test. As indicated in Fig. 23, some specific details are as follows:

(1) The automated top-coal caving technology should be determined by simulation optimizing. From section 4.2 of the manuscript, the automated four-round coal caving is the optimal technology, which comprehensively considers the movement of coal-rock interface, rock mixed rate, top-coal recovery rate and transport efficiency. Based on this, the automated coal caving rounds of the engineering site can be obtained.
(2) The coal drawing test in field should be carried out in the middle of working face to obtain the coal drawing time of single drawing opening, which is considered as the maximum value of automated coal drawing time for each coal drawing opening.

(3) Based on the principle of "rocks appear, close the opening", the coal drawing operations of working face are executed in sequence to get total coal drawing time of entirely working face. The average coal drawing time of every drawing opening is determined by the ratio of total coal caving time to the number of coal drawing supports. Meanwhile, the average coal drawing time of every drawing opening should be less than the maximum value of automated coal drawing time for each drawing opening. Then, the coal drawing time of single drawing opening in every round is obtained by the ratio of single drawing opening time to the number of coal drawing rounds.
(4) The obtained coal drawing time in automated multi-round coal drawing should be corrected by the field equipment, which not only to obtain the higher transport efficiency of top-coal, but also to ensure that the armored face conveyor is not overloaded. Meanwhile, the total automated coal drawing time should be also satisfied with the coal production schedule to achieve the more efficient and coordinated coal mining.

5. Conclusions

The coupled calculation approach of particle and block elements based on the CDEM is presented and verified, then is used to simulate the top-coal breaking and drawing processes under the interaction between hydraulic support and surrounding rocks. The constitutive model of hydraulic support is introduced into the CDEM to analyze the top-coal drawing mechanism, and the Bergmark–Roos model is extended into the collaborative coal drawing of multiple supports to optimize the automated top-coal caving technology. Furthermore, an automated coal caving technology is put forward via comparison analyses of decisive parameters influencing automated top-coal caving. Taking the Tongxin Coal Mine as an engineering example, the following conclusions can be drawn:

(1) Based on the calculation approach coupled with particle element and block element, the continuous-discontinuous phenomena of top-coal caving and drawing process can be well characterized. In the initial mining stage, the subsidence amount of overlying strata is relatively smaller, and no instability failure occurs in the main roof strata. Factors determining the shape of the drawing body are the hydraulic support, intact top-coal and large immediate roof rock masses. The drawing body shape firstly resembles an incomplete ellipsoid cut by the tail beam in the initial coal drawing process, while the final drawing body shape presents as an irregularly deflected ellipsoid. During different support-moving cycles, the coal-rock masses are cracking, dislocating and flowing. Subsequently, the top-coal is drawn out by the drawing opening. Furtherly, the coal-rock structure significantly affects the coal drawing amount and support resistance.
(2) On the cross-section parallel to the coal face, the horizontal stress acting on the broken top-coal near the drawing opening is an advantage in the first stage of coal drawing, while the stress hinders the top-coal drawing in second stage. The drawing body shape on the cross-section parallel to the coal face is not affected by support and presents an approximate ellipsoidal shape, which is basically in accordance with the Bergmark–Roos theory model. The top-coal drawing theoretical model is also available for studying the top-coal drawing process of 100 drawing openings.
(3) The impact of adjacent drawing openings on automated coal caving is smaller than traditional coal caving, the standard deviation of the coal drawing amount in automated one-round coal caving (1.83 m^2) is less than that in traditional coal caving (8.23 m^2), and the coal drawing amount from each drawing window is more uniform. Therefore, the coal drawing operations are simpler, and the transport efficiency of the scraper conveyer is higher than in traditional top-coal caving. The coal-rock interface above the drawing opening becomes gradually smoother as the total rounds of automated top-coal caving increase from 2 to 6, and the layered top-coal is drawn out. Furthermore, the average recovery rate for the multi-round coal caving technique remains at 79.4% and the rock mixed rate is less than 1%. This comparison illustrates that automated four-round coal caving technology is the optimal technology, because its comprehensive benefits are the best, which fully considers the rock mixed rate, top-coal recovery rate and transport efficiency of the scraper conveyer. Based on this, the method of determining automated coal drawing time by the combination of simulation and in-site test is proposed for the practical mining.

Acknowledgments

This work was supported by the National Key R&D Program of China (Grant No. 2018YFC0604502); the project of automated top-coal caving system research funded by Datong Coal Mine Group; and National Natural Science Foundation of China (Grant No. 51708513). The authors gratefully acknowledge Professor Yingchun Cai in Zhengzhou University, Dr. Lingling Xu in Southeast University and Dr. Shen Wang in Henan Polytechnic University, who provide language help and writing assistance.

References

1. Wang JC, Yang SL, Li Y, et al. Caving mechanisms of loose top coal in longwall top coal caving mining method. *Int J Rock Mech Min Sci.* 2014;71:160–170 https://doi.org/10.1016/j.ijrmms.2014.04.024.
2. Yang SL, Zhang JW, Chen Y, et al. Effect of upward angle on the drawing mechanism in longwall top coal caving mining. *Int J Rock Mech Min Sci.* 2016;85:92–101 https://doi.org/10.1016/j.ijrmms.2016.03.004.
3. Xie YS, Zhao YS. Numerical simulation of the top coal caving process using the discrete element method. *Int J Rock Mech Min Sci.* 2009;46:983–991 https://doi.org/10.1016/j.ijrmms.2009.03.005.
4. Yasitli NE, Unver B. 3D numerical modeling of longwall mining with top coal caving. *Int J Rock Mech Min Sci.* 2005;42:219–235 https://doi.org/10.1016/j.ijrmms.2004.08.007.
5. Ediz IG, Dixon-Hardy DW, Akcakoca H, et al. Application of retreating and caving longwall (top coal caving) method for coal production at GLE Turkey. *Min Technol.* 2013;115:41–48 https://doi.org/10.1179/174328606X103586.
6. Wang JC. Engineering practice and theoretical progress of top coal caving mining technology in China. *J China Coal Soc.* 2018;43:43–51 https://doi.org/10.13225/j.cnki.jccs.2017.4101.
7. Wang GF, Pang YH, Ma Y, et al. Automated mining technology and equipment for fully-mechanized caving mining with large mining height in extra-thick coal seam. *Coal Eng.* 2018;50:1–6 https://doi.org/10.11799/ce201801001.
8. Ma Y. Study on automatic top coal caving system in fully-mechanized coal caving face. *Coal Sci Technol.* 2013;41:22–24 https://doi.org/10.13199/j.cnki.cst.2013.11.019.
9. Wang GF, Pang YH, Ren HW, et al. Coal safe and efficient mining theory, technology and equipment innovation practice. *J China Coal Soc.* 2018;43:903–913 https://doi.org/10.13225/j.cnki.jccs.2017.1705.
10. Wang GF, Wang H, Ren HW, et al. 2025 scenarios and development path of intelligent coal mine. *J China Coal Soc.* 2018;43:295–305 https://doi.org/10.13225/j.cnki.jccs.2018.0152.
11. Wu J, Zhang Y. Study on the basic theory of longwall top coal caving system. *J China Univ Min Technol.* 1998;27:331–335 http://www.cnki.com.cn/Article/CJFDTotal-ZGKD804.000.htm.
12. Yan SH, Wu J. Analysis of top coal movement and damage characteristics in top coal caving. *J China Coal Soc.* 1996;15:155–162 http://www.cnki.com.cn/Article/CJFDTotal-YSLX602.010.htm.
13. Wu J. Theory and practice of sub-level caving method in China. *J China Coal Soc.* 1991;3:1–11 https://doi.org/10.13225/j.cnki.jccs.1991.03.001.
14. Wang JC, FU Q. The loose medium flow field theory and its application on the longwall top coal caving. *J China Coal Soc.* 2002;27:337–341 https://doi.org/10.3321/j.issn:0253-9993.2002.04.001.
15. Wang JC, Li ZG, Chen YJ, et al. The experimental study of loose medium flow field on the longwall top coal caving. *J China Coal Soc.* 2004;29:260–263 https://doi.org/10.13225/j.cnki.jccs.2004.03.002.
16. Wang JC, Zhang JW, li ZL. A new research system for caving mechanism analysis and its application to sublevel top coal caving mining. *Int J Rock Mech Min Sci.* 2016;88:273–285 https://doi.org/10.1016/j.ijrmms.2016.07.032.
17. Wang JC, Song ZY, Zhang JW, et al. Three-dimensional experimental study of loose top coal drawing law for longwall top coal caving mining technology. *J Rock Mech and Geo Eng.* 2015;7:318–326 https://doi.org/10.1016/j.jrmge.2015.03.010.
18. Wang JC, Wei LK, Zhang JW, et al. 3-D numerical simulation on the top coal movement law under caving mining technique. *J China Coal Soc.* 2013;38:1905–1911 https://doi.org/10.13225/j.cnki.jccs.2013.11.013.

19. Khanal M, Adhikary D, Balusu R. Evaluation of mine scale longwall top coal caving parameters using continuum analysis. *Min Sci Technol.* 2011;21(6):787–796 https://doi.org/10.1016/j.mstc.2011.06.027.
20. Vakili A, Hebblewhite BK. A new cavability assessment criterion for Longwall Top Coal Caving. *Int J Rock Mech Min Sci.* 2010;47:1317–1329 https://doi.org/10.1016/j.ijrmms.2010.08.010.
21. Li SH, Zhao MH, Wang YN, et al. A new numerical method for DEM-block and particle model. *Int J Rock Mech Min Sci.* 2004;41 436-436 https://doi.org/10.1016/j.ijrmms.2003.12.076.
22. Wang LX, Li SH, Zhang GX, et al. A GPU-based parallel procedure for nonlinear analysis of complex structures using a coupled FEM/DEM approach. *Math Probl Eng.* 2013:618980 https://doi.org/10.1155/2013/618980.
23. Ma K, Tang CA, Wang LX, et al. Stability analysis of underground oil storage caverns by an integrated numerical and microseismic monitoring approach. *Tunn Undergr Space Technol.* 2016;54:81–91 https://doi.org/10.1016/j.tust.2016.01.024.
24. Ju Y, Liu P, Chen JL, et al. CDEM-based analysis of the 3D initiation and propagation of hydrofracturing cracks in heterogeneous glutenites. *J Nat Gas Sci Eng.* 2016;35:614–623 https://doi.org/10.1016/j.jngse.2016.09.011.
25. Liu C, Li HM, Jiang DJ. Numerical simulation study on the relationship between mining heights and shield resistance in longwall panel. *J China Univ Min Technol.* 2017;27(2):293–297 https://doi.org/10.1016/j.ijmst.2017.01.017.
26. Li HM, Zhang QL, Liu C, et al. Analysis on overburden strata movement and mine strata pressure behavior of high cutting mining in ultra thick seam. *Coal Sci Technol.* 2017;45(1):27–33 https://doi.org/10.13199/j.cnki.cst.2017.01.005.
27. Feng C, Li SH, Liu XY. A procedure for transiting FEM into DEM and its application. *Rock Soil Mech.* 2015;36(4):1027–1034 https://doi.org/10.16285/j.rsm.2015.04.017.
28. Potyondy DO, Cundall PA. A bonded-particle model for rock. *Int J Rock Mech Min Sci.* 2004;41:1329–1364 https://doi.org/10.1016/j.ijrmms.2004.09.011.
29. Xu GW, He C, Chen ZQ, et al. Transverse isotropy of phyllite under Brazilian tests: laboratory testing and numerical simulations. *Rock Mech Rock Eng.* 2017;51(4):1111–1135 https://doi.org/10.1007/s00603-017-1393-x.
30. Wang JC, Song ZY, Zhang JW, et al. Theoretical model of drawing body in LTCC mining. *J China Coal Soc.* 2016;41:352–358 https://doi.org/10.13225/j.cnki.jccs.2015.1750.
31. Kuchta ME. A revised form of the Bergmark–Roos equation for describing the gravity flow of broken rock. *Miner Resour Eng.* 2002;11:349–360 https://doi.org/10.1142/S0950609802001002.
32. Melo F, Vivanco F, Fuentes C, et al. On drawing body shapes: from Bergmark–Roos to kinematic models. *Int J Rock Mech Min Sci.* 2007;44:77–86 https://doi.org/10.1016/j.ijrmms.2006.04.010.
33. Karekal S, Das R, Mosse L, et al. Application of a mesh-free continuum method for simulation of rock caving processes. *Int J Rock Mech Min Sci.* 2011;48(5):703–711 https://doi.org/10.1016/j.ijrmms.2011.04.011.
34. Konak, et al. Determination of immediate roof at Kutahya-Omerler coal basin Turkey. *J Min Sci.* 2006;42:157–170 https://doi.org/10.1007/s10913-006-0043-6.
35. Whittaker BN, Pasamehmetoglu AG. Ground tilt in relation to subsidence in Longwall mining. *Int J Rock Mech Min Sci.* 1981;18(4):321–329 https://doi.org/10.1016/0148-9062(81)91196-7.
36. Singh KB, Singh TN. Ground movements over longwall workings in the Kamptee coalfield, India. *Eng Geol.* 1998;50:125–139 https://doi.org/10.1016/S0013-7952(98)00005-2.
37. Sheorey PR, Loui JP, Singh KB, et al. Ground subsidence observations and a modified influence function method for complete subsidence prediction. *Int J Rock Mech Min Sci.* 2000;37(5):801–818 https://doi.org/10.1016/S1365-1609(00)00023-X.
38. Marschalko M, Yilmaz I, Kristkova V, et al. Determination of actual limit angles to the surface and their comparison with the empirical values in the Upper Silesian Basin (Czech Republic). *Eng Geol.* 2012;124:130–138 https://doi.org/10.1016/j.enggeo.2011.10.010.
39. Marschalko M, Yilmaz I, Bednarik M, et al. Influence of underground mining activities on the slope deformation genesis: doubrava Vrchovec, Doubrava Ujala and Staric case studies from Czech Republic. *Eng Geol.* 2012;147–148:37–51 https://doi.org/10.1016/j.enggeo.2012.07.014.
40. Marschalko M, Yilmaz I, Bednarik M, et al. Variations in the building site categories in the underground mining region of Doubrava (Czech Republic) for land use planning. *Eng Geol.* 2011;122:169–178 https://doi.org/10.1016/j.enggeo.2011.05.008.
41. Aksoy CO, Kose H, Onargan T, et al. Estimation of limit angle by laminated displacement discontinuity analyses in soma coal field, Western Turkey. *Int J Rock Mech Min Sci.* 2004;41(4):547–556 https://doi.org/10.1016/j.ijrmms.2003.01.002.